

On the Linear Approximation of Velocity and Density Profiles in the Problem of Baroclinic Instability

E. S. BENILOV* AND P. V. SAKOV

Department of Mathematics, University of Tasmania, Launceston, Australia

27 July 1997 and 2 September 1998

ABSTRACT

The linear approximation of density and velocity profiles is compared to more realistic models with vertically inhomogeneous density gradients and nonzero anomalous vorticity (i.e., the nonplanetary part of potential vorticity). Calculations based on the parameters of “real life” currents in the Northern Pacific demonstrate that these effects, acting together, can make baroclinic instability 2.5–6 times stronger and dramatically expand the spectral range of unstable disturbances toward the short-wave region (by a factor of more than 20–30).

1. Introduction

The linear approximation of density and velocity profiles is widely used for the description of baroclinic instability. Its main advantage is simplicity, as linearly stratified flows are described by a “solvable” normal-mode equation. At the same time, the linear approximation allows one to elucidate the basic physics of baroclinic instability (see Charney 1947; Eady 1949; Green 1960).

Still, the linear approximation seems to have two shortcomings. First, it reduces potential vorticity to its planetary part, as the *anomalous* vorticity (i.e., the nonplanetary part) vanishes identically for all linearly stratified flows. This should certainly be seen as a drawback, as for many real-life oceanic currents anomalous vorticity is considerably greater than the planetary vorticity, and omission of the former can result in a significant error in the parameters of baroclinic instability. Second, the global stability of a flow is, generally, determined by the stability of its least stable layer—thus, any perturbation of the homogeneous (linear) density stratification must strengthen the instability.

In this paper, we estimate the influence of nonzero anomalous vorticity and inhomogeneous density stratification on the parameters of baroclinic instability for a number of “real life” currents in the northern Pacific.

It is demonstrated that the two effects, acting together, may increase the growth rate by the order of magnitude and dramatically widen the spectrum of unstable disturbances. Unlike predictions of the linear model, the “modified” results agree with oceanic observations of baroclinic instability (see section 5 below).

It should be mentioned that there is a large body of work dealing with the application of the equation of baroclinic instability to the real ocean, of which we cite one of the earliest ones (Gill et al. 1974) and one of the most recent ones (Killworth et al. 1997). In these papers, the parameters of baroclinic instability were computed for many oceanic currents. In order to emphasize the difference between these papers and the present note, we remark that the question we ask is not “what are the parameters of baroclinic instability” but rather “which features of oceanic currents are responsible for the parameters of baroclinic instability that we observe.”

2. Mathematical formulation

In addition to the aforementioned shortcomings, linear profiles of density and velocity imply that the flow penetrates down to the oceanic bottom, which clearly contradicts observations (e.g., Roden 1975). We shall use a model assuming that the flow is localized in an “active” layer of depth H_a , while in the “passive” layer we have

$$\rho(z) = \rho_0, \quad u(z) = 0 \quad \text{for } z \leq -H_a,$$

where $\rho(z)$ and $u(z)$ are the density and velocity profiles, and z is the vertical spatial variable (see Fig. 1). We shall also assume that the ocean is horizontally homogeneous (no dependency on y). In the active layer, the

* Current affiliation: Department of Mathematics, University of Limerick, Limerick, Ireland.

Corresponding author address: Dr. Eugene S. Benilov, Department of Mathematics, University of Limerick, Limerick, Ireland.
E-mail: eugene@maths.warwick.ac.uk

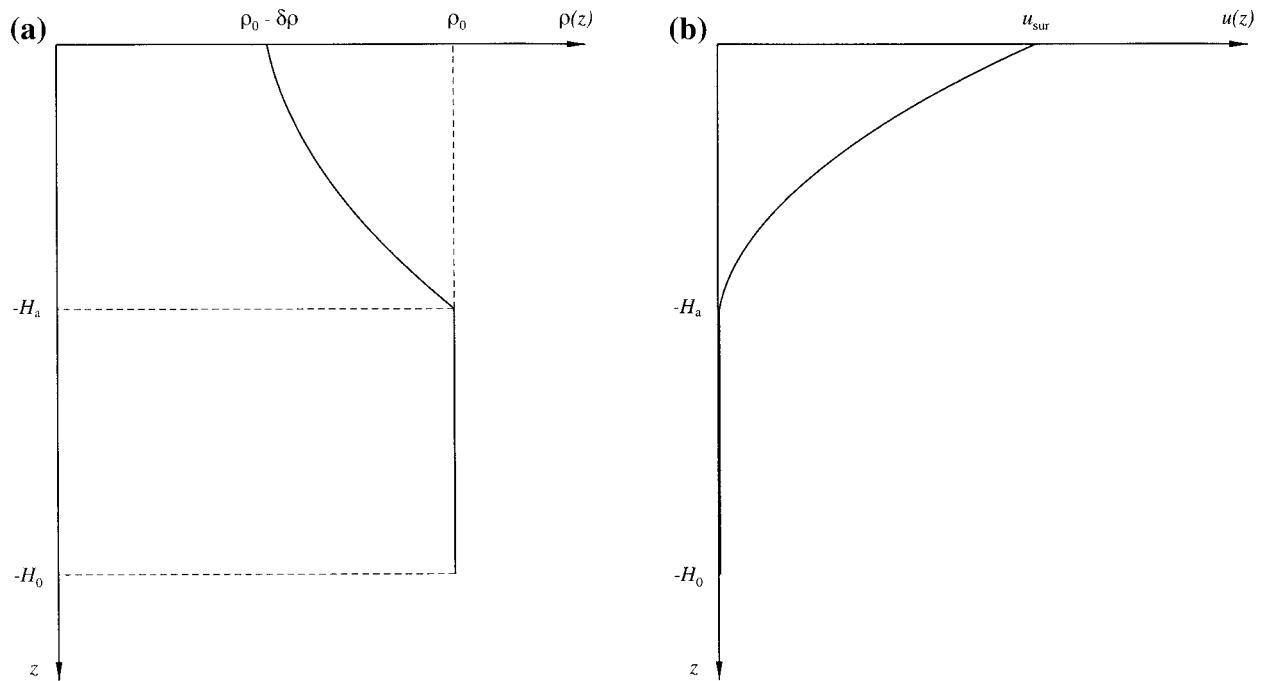


FIG. 1. The (a) density and (b) velocity profiles.

stability of a normal mode with wavenumber k and phase speed c is governed by (e.g., Pedlosky 1987, p. 514)

$$\frac{f^2 \rho_0}{g} \left[\frac{(u-c)^2}{\rho_z} \phi_z \right]_z + [k^2(u-c)^2 - \beta(u-c)] = 0, \quad (1)$$

where g is the acceleration due to gravity, ρ_0 is the passive layer's density (the Boussinesq approximation implied), f and β are the Coriolis and beta parameters respectively, k is the wavenumber of the disturbance, c is its phase speed, and $\phi(z)$ describes the vertical structure of the mode. The streamfunction of the disturbance is given by

$$\psi(x, y, z, t) = \phi(z)[u(z) - c] \exp[ik^{(x)}(x - ct) + ik^{(y)}y],$$

where $(k^{(x)}, k^{(y)})$ is the horizontal wavevector of the disturbance ($k^{(x)2} + k^{(y)2} = k^2$). In the passive layer ρ_z vanishes, and the first term in Eq. (1) becomes singular, which makes it impossible to solve this equation numerically. In order to bypass this difficulty, one should resolve the structure of the disturbance in the passive layer *analytically* and formulate a boundary condition that "parameterizes" the influence of the passive layer:

$$-\frac{f^2 \rho_0}{g} \frac{c}{\rho_z} \phi_z = (H_0 - H_a)(k^2 c + \beta) \phi \quad \text{at } z = -H_a, \quad (2)$$

where H_0 is the total depth of the ocean. Boundary condition (2) has been derived in a more general form by Benilov (1994, 1995); in order to make the present paper self-contained, a simple derivation of (2) is given in appendix A. In most cases considered in this paper,

the depth of the active layer is relatively small, and we could, in principle, use the reduced gravity model employed previously in similar problems by Fukamachi et al. (1995) and Beron-Vera and Ripa (1997, manuscript submitted to *J. Fluid Mech.*, hereafter BVR).¹ However, we shall use the *exact* boundary condition (2), which is just as simple computationally. Another difference with the paper by BVR is that the latter also includes a velocity jump across the interface. As none of the real-life examples (considered below) includes a rapid change of velocity in/near its passive layer, we shall assume that the velocity profile is continuous; that is,

$$u(-H_a) = 0.$$

Finally, at the surface of the ocean, we impose the rigid-lid condition:

$$\phi_z = 0 \quad \text{at } z = 0. \quad (3)$$

Equations (1)–(3) form an eigenvalue problem for c . If $\text{Im}c \neq 0$, the disturbance with the corresponding value of k is unstable with the growth rate $(k^{(x)} \text{Im}c)$. Equation (1) was solved using the eighth-order Dormand–Prince method with automatic adjustment of the step length (Dormand and Prince 1980; see also Hairer et al. 1993). If the complex part of c was small and the critical level was located close to the real axis of the complex z plane

¹ Within the framework of this model, the active layer–passive layer interface is replaced by a free surface, which enables one to consider the boundary value for normal modes only in the upper (active) layer of the ocean.

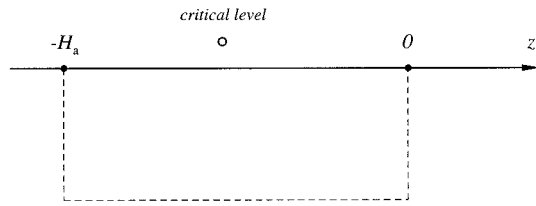


FIG. 2. The path of integration (dashed line) of Eq. (1) on the complex z plane for the cases where the critical level is located close to the real axis.

(say, from above), the path of integration was shifted (downward) to bypass the singularity and thus improve the accuracy (see Fig. 2). The solution was “shot” from the lower boundary condition (2) and the value of $\phi_z(0)$ was fed to the root-finding routine based on the Newton–Raphson method, yielding a solution for c .

3. Physical formulation

Consider a model of stratification with quadratic approximation of density and velocity fields:

$$\frac{\rho - \rho_0}{\rho_0} = \sigma_1(z + H_a) + \sigma_2(z + H_a)^2, \\ u = u_1(z + H_a) + u_2(z + H_a)^2. \quad (4)$$

The undetermined constants $\sigma_{1,2}$ and $u_{1,2}$ will be adjusted to describe certain real-life currents in the northern Pacific. In what follows, we shall use the following notation:

- K: Kuroshio;
- SA: subarctic frontal current;
- ST₁: subtropical frontal current, northern jet;
- ST₂: subtropical frontal current, middle jet; and
- ST₃: subtropical frontal current, southern jet.

The parameters of these currents, extracted from Roden (1975), are shown in Table 1.

The simplest model of the kind (4) assumes both $\rho(z)$ and $u(z)$ to be linear, which will be referred to as the LL model. In this case,

$$\sigma_2 = 0, \quad u_2 = 0, \quad (5)$$

and σ_1 and u_1 were determined using the measured depth of the active layer H_{a*} , the surface (maximum) value u_{sur*} of the velocity, and the density change $(\delta\rho/\rho_0)_*$ through the active layer

$$\sigma_1 = -\frac{(\delta\rho/\rho_0)_*}{H_{a*}}, \quad u_1 = \frac{u_{sur*}}{H_{a*}}, \quad (6)$$

where the asterisk marks the “real life” (observed by Roden 1975) parameters. The LL model is relatively crude and, in particular, fails to provide the “correct” value of the slope of the active layer–passive layer interface. This important characteristic of the flow is given by the formula

TABLE 1. Parameters of frontal currents in the northern Pacific: θ is the latitude, H_{0a} is the total depth of the ocean, H_{a*} is the depth of the active layer. $(\delta\rho/\rho_0)_* = [\rho_*(-H_{a*}) - \rho_*(0)]/\rho_{0*}$ is the relative density change through the active layer, $u_{sur*} = u_*(0)$ is the surface velocity, L_* is the width of the current, and δH_{a*} is the corresponding (transverse) variation of the depth of the active layer.

	K	SA	ST ₁	ST ₂	ST ₃
θ (°N)	38	42	30	29	28
H_{0a} (m)	5500	5500	5500	5500	5500
H_{a*} (m)	600	500	350	350	500
$(\delta\rho/\rho_0)_* \times 10^3$	1.7	1.3	1.3	1.3	1.8
u_{sur*} (m s ⁻¹)	0.55	0.40	0.20	-0.15	0.45
L_* (km)	145	200	210	120	150
δH_{a*} (m)	200	300	140	-60	140

$$s = -\frac{f\rho_0}{g} \frac{u_z(-H_a)}{\rho_z(-H_a)}, \quad (7)$$

derived in appendix B. For the LL model,

$$s = -\frac{f}{g} \frac{u_1}{\sigma_1},$$

which does not necessarily match the observed value

$$s_* = \frac{\delta H_{a*}}{L_*},$$

where L_* is the observed width of the current and δH_{a*} is the corresponding (transverse) change in the depth of the active layer. For the Kuroshio Current, for example, the LL model gives $s = 2.96 \times 10^{-3}$, while the actual value (following from Roden’s data, see Table 1) is $s_* = 1.38 \times 10^{-3}$.

In order to obviate this drawback, we also considered a model with a linear approximation of density and quadratic approximation of velocity (which will be referred to as the LQ model). The density stratification remained the same as in the LL model:

$$\sigma_1 = -\frac{(\delta\rho/\rho_0)_*}{H_{a*}}, \quad \sigma_2 = 0, \quad (8)$$

while the velocity profile was adjusted to provide the “correct” values for both u_{sur*} and s_* :

$$u_1 = -\frac{g\sigma_1 s_*}{f}, \quad u_2 = \frac{u_{sur*}}{H_a^2} - \frac{u_1}{H_a}. \quad (9)$$

Finally, we considered the general case of quadratic approximation for both $\rho(z)$ and $u(z)$ (which will be referred to as the QQ model). In comparison with the LQ model, this approximation has an extra degree of freedom (σ_2), which cannot be fixed using the “global” characteristics of the flow (i.e., parameters in Table 1). Unfortunately, Roden (1975) supplied no precise information on the vertical structure of the density field (in which case σ_2 could have been adjusted through a least squares fit). Thus, we had to model the inhomogeneity of density gradient in the active layer on a more or less

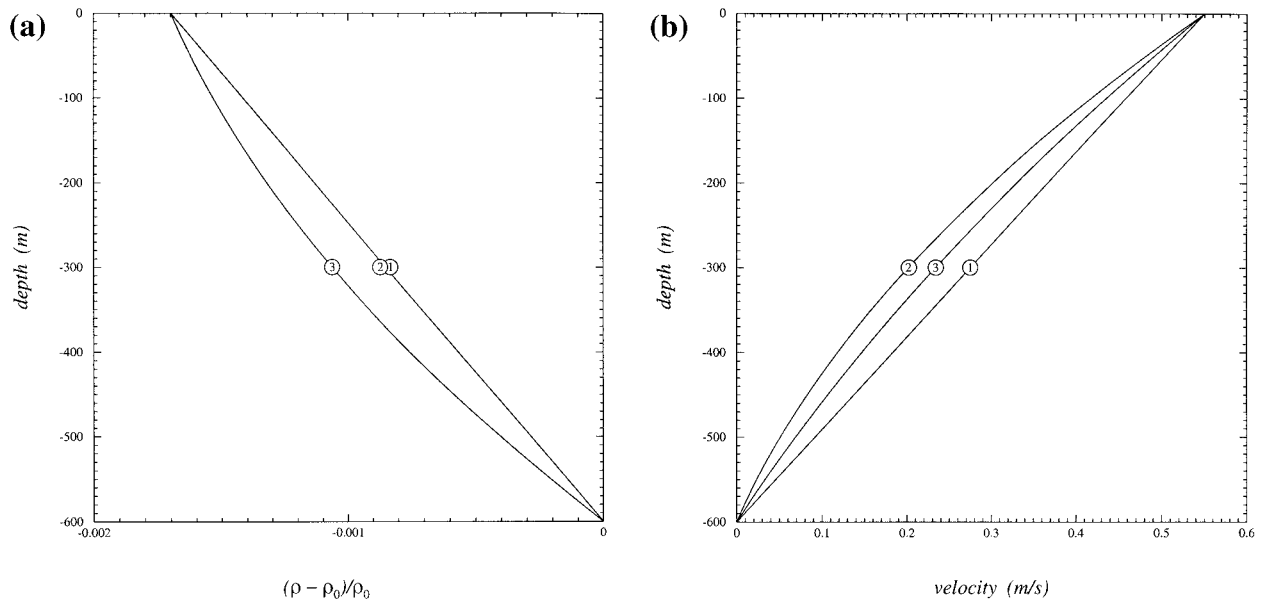


FIG. 3. The three models of stratification for the Kuroshio frontal current: 1) = LL model (5)–(6), 2) = LQ model (8)–(9), and 3) = QQ model (10)–(11); (a) density stratification (observe that the LL and LQ models coincide), and (b) velocity stratification.

ad hoc basis. We assumed that the density gradient at the lower boundary of the active layer was, say, three times greater than that at the surface of the ocean:

$$\sigma_1 = -\frac{3}{2} \frac{(\delta\rho/\rho_0)_*}{H_{a*}}, \quad \sigma_2 = \frac{1}{2} \frac{(\delta\rho/\rho_0)_*}{H_{a*}^2}, \quad (10)$$

(which was supposed to model weakening of the density stratification in the upper mixed layer). Adjusting $u_{1,2}$ to provide the correct values of u_{sur*} and s_* , we obtain

$$u_1 = -\frac{g\sigma_1 s_*}{f}, \quad u_2 = \frac{u_{sur*}}{H_a^2} - \frac{u_1}{H_a}. \quad (11)$$

Thus, we have three different models of stratification: (5)–(6), (8)–(9), and (10)–(11). In what follows, we shall apply them to the currents represented in Table 1 and compare the results.

Interestingly enough, the three models do not look significantly different (see Fig. 3), yet they result in completely different parameters of baroclinic instability.

4. Results

The main characteristic of a hydrodynamic instability is its maximum growth rate:

TABLE 2a. The e -folding times of frontal currents in the northern Pacific, computed through the LL model (5)–(6), LQ model (8)–(9), and QQ model (10)–(11).

	K	SA	ST ₁	ST ₂	ST ₃
τ_{LL} (days)	9	10	stable	27	34
τ_{LQ} (days)	5	5	15	17	9
τ_{QQ} (days)	3	4	10	12	6

$$\gamma = \max\{k^{(v)} \text{Im}c(k)\},$$

and the corresponding wavenumber k_m (or, equivalently, the e -folding time $\tau = 1/\gamma$ and the wavelength $\lambda_m = 2\pi/k_m$). The values of these parameters computed for the aforementioned currents and models are presented in Tables 2a,b. Another important parameter of baroclinic instability is its spectral range, usually characterized by long/short-wave cutoffs. In our case, however, the long-wave cutoff corresponds to unrealistically long waves (longer than 400–600 km); that is, we can safely assume that all long waves are weakly unstable. The short-wave cutoff, in turn, simply does not exist, as $c(k)$ approaches zero asymptotically as $k \rightarrow \infty$. Thus, we shall assume that the cutoffs correspond to the disturbances with growth rates, say, three times smaller than the maximum growth rate:

$$k_{\pm} \text{Im}c(k_{\pm}) = \frac{1}{3} \gamma, \quad k_- < k_m < k_+,$$

(see the schematic in Fig. 4). The corresponding wavelengths $\lambda_{\pm} = 2\pi/k_{\pm}$ computed for the aforementioned currents and models are presented in Table 3.

The results in Tables 2 and 3 can be summarized as follows:

TABLE 2b. The wavelengths of maximum growth of frontal currents in the northern Pacific computed through the LL model (5)–(6), LQ model (8)–(9), and QQ model (10)–(11).

	K	SA	ST ₁	ST ₂	ST ₃
$(\lambda_m)_{LL}$ (km)	300	230	stable	230	370
$(\lambda_m)_{LQ}$ (km)	105	80	90	95	140
$(\lambda_m)_{QQ}$ (km)	70	55	60	70	90

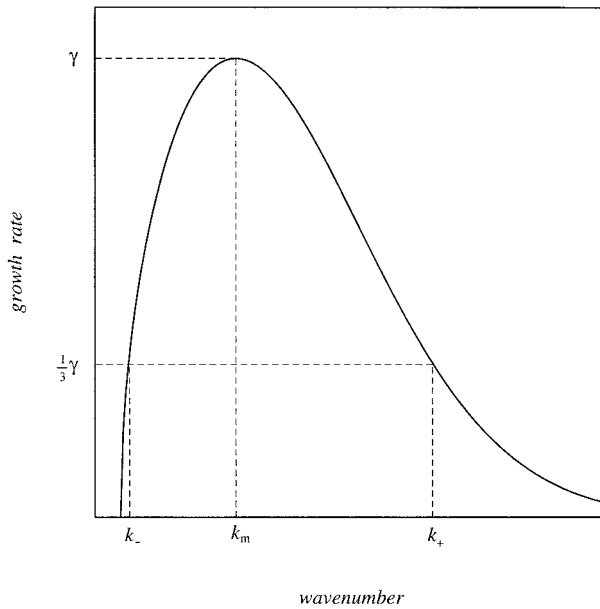


FIG. 4. Characteristics of baroclinic instability: γ and k_m are the maximum growth rate and the corresponding wavenumber and k_- and k_+ are the long/short-wave boundaries of the instability.

- (i) Nonzero anomalous vorticity (which makes the difference between the LL and LQ models)
 - increases the maximum growth rate of the instability by a factor of approximately 1.5–4 (see Table 2a),
 - shifts the most unstable harmonic toward the short-wave region by a factor of approximately 2.5–4 (see Table 2b),
 - shifts the long-wave boundary of the instability toward the short-wave region by a factor of approximately 1.2–1.5 (see Table 3),
 - shifts the short-wave boundary of the instability toward the short-wave region by a factor of approximately 7–9 (see Table 3).
- (ii) Vertical inhomogeneity of density stratification (which makes the difference between the LQ and QQ models)
 - increases the maximum growth rate of the instability by a factor of approximately 1.5 (see Table 2a),
 - shifts the most unstable harmonic toward the

short-wave region by a factor of approximately 1.5 (see Table 2b),

- shifts the long-wave boundary of the instability toward the short-wave region by a factor of approximately 1–1.5 (see Table 3),
- shifts the short-wave boundary of the instability toward the short-wave region by a factor of more than 2–4 (see Table 3).

Thus, the combined effect of *nonzero anomalous vorticity* and *inhomogeneous density stratification* makes baroclinic instability 2.5–6 times *stronger* and dramatically expands the spectral range of unstable disturbances toward the *short-wave region* (by a factor of more than 20–30).

This conclusion is illustrated by Fig. 5, where we show the growth rates of baroclinic instability of the Kuroshio Current (as an example of an eastward flow) and the subtropical front’s middle jet ST_2 (as an example of a westward flow). In both cases, the growth rate computed using the most realistic QQ model seems to have no spectral gap between the Rossby wave and internal-wave ranges of disturbances.

5. Discussion

1) The main reason for such a strong difference between the linear (LL) and nonlinear (LQ, QQ) models of stratification lies in the structure of potential vorticity:

$$\frac{f^2 \rho_0}{g} \left(\frac{\Psi_z}{\rho_z} \right) + \beta y, \tag{12}$$

where Ψ is the streamfunction of the basic flow. Taking into account that, for currents without horizontal shear,

$$\Psi = -yu(z), \tag{13}$$

we estimate the ratio of the first (anomalous vorticity) term in (12) to the second (planetary vorticity) term:

$$\mu \sim \frac{\text{anomalous vorticity}}{\text{planetary vorticity}} \sim \frac{u_{\text{sur}*}}{\beta R_d^2}, \tag{14}$$

where $u_{\text{sur}*}$ is the surface (maximum) velocity and R_d is the deformation radius based on the depth of the active layer:

$$R_d = \frac{\sqrt{(\delta\rho/\rho_0)_* g H_{a*}}}{f}. \tag{15}$$

Estimating μ for the aforementioned currents in the

TABLE 3. The spectral ranges (wavelengths) of unstable disturbances for frontal currents in the northern Pacific, computed through the LL model (5)–(6), LQ model (8)–(9), and QQ model (10)–(11). The asterisk indicates that the corresponding short-wave cutoff is less than 15 km.

	K	SA	ST ₁	ST ₂	ST ₃
$(\lambda_+ - \lambda_-)_{LL}$ (km)	210–600	170–500	stable	180–370	320–450
$(\lambda_+ - \lambda_-)_{LQ}$ (km)	30–440	20–350	20–230	22–320	35–360
$(\lambda_+ - \lambda_-)_{QQ}$ (km)	*–290	*–210	*–190	*–320	*–300

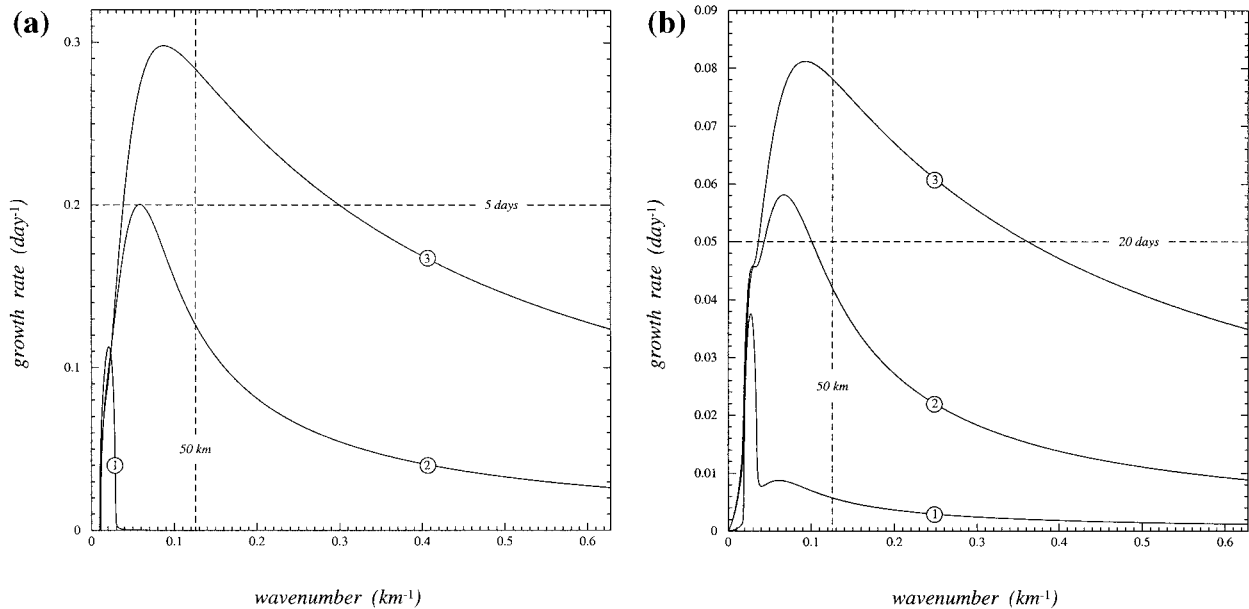


FIG. 5. Growth rate of baroclinic instability. 1) = LL model (5)–(6), 2) = LQ model (8)–(9), and 3) = QQ model (10)–(11). (a) Kuroshio frontal current (dashed lines show the “reference values” of 5 days for the e -folding time and 50 km for the wavelength of disturbance), and (b) subtropical frontal current (dashed lines show the reference values of 20 days for the e -folding time and 50 km for the wavelength of disturbance).

northern Pacific, we see that the anomalous vorticity is, typically, 10–30 times greater than the planetary vorticity (see Table 4). Thus, it comes as no surprise that the LL model, having zero anomalous vorticity,² differs significantly from the (more realistic) nonlinear approximations having nonzero anomalous vorticity.

Finally, we shall compare the deformation radius R_d (see Table 5) with the wavelength of maximum growth computed through the (most realistic) QQ model (Table 2b, the last row). It turned out that, for all currents considered, the latter is almost precisely two times larger than the former. This agrees with the generally accepted hypothesis that the spatial scale of baroclinic instability is of the order of R_d . At the same time, the linear model of stratification produces a much larger than R_d spatial scale.

2) We shall also test the results obtained here against observations. Generally speaking, there is no reason for the real ocean to be linearly stratified, hence the LQ and QQ models should fare better than the LL model. We shall compare theoretical results to those obtained by

Lee and Eriksen (1996), who estimated the characteristic timescale of variability of subtropical fronts to be about 10 days. Evidently, this estimate agrees with the QQ model better than with either of the other two (see columns ST_{1–3} in Table 2a). At the same time, the LL model is completely off the mark. Unfortunately, neither Lee and Eriksen (1996) nor other authors provide much information on the spatial structure of disturbances in midoceanic fronts, thus we were unable to compare our results in Table 2b with observations. We were able, however, to make an indirect comparison between theoretically predicted wavelengths and the size of oceanic rings (which are a product of frontal instability and thus should inherit its spatial scale). We used the data collected by Olson (1991), including three rings observed in the Kuroshio frontal current. Their radii were 60, 75, and 105 km, which again suggests that the two nonlinear models fare better than the linear one.

We have also made some estimates for near-coastal fronts. Following Fukamachi et al. (1995), we assumed that

$$\theta = 43^\circ, \quad H_{0*} = 250 \text{ m}, \quad H_{a*} = 50 \text{ m},$$

$$\frac{\delta\rho}{\rho_0} = 0.75 \times 10^{-3}, \quad u = 0.5 \text{ m s}^{-1}.$$

Using these parameters, the LL model yields

$$\tau_{LL} \approx 1 \text{ day}, \quad (\lambda_m)_{LL} \approx 60 \text{ km}.$$

These results agree well with the predictions of the two-layer model (Phillips 1954), but at the same time disagree with observations. Specifically, the spatial scale

² Observe that the first term in (12) vanishes for the LL model [i.e., for (13), (4) with $\sigma_2 = 0$, $u_2 = 0$].

TABLE 4. The effective ratio (14) of the anomalous and planetary vorticities for frontal currents in the northern Pacific.

	K	SA	ST ₁	ST ₂	ST ₃
μ	25	34	12	8	11

TABLE 5. The deformation radius (15) for frontal currents in the northern Pacific.

	K	SA	ST ₁	ST ₂	ST ₃
R_d (km)	35	25	30	30	45

$(\lambda_m)_{LL}$ is 2–3 times larger than a typical observed value (see Fukamachi et al. 1995 and references therein). The e -folding time τ_{LL} does agree with observations, but we cannot trust it, as it is comparable to f^{-1} —which indicates that the instability is ageostrophic. (Note that the LQ and QQ models give more realistic results, which cannot be trusted, however, for the same reason as the LL results.) The instability of fronts with steeply tilted isopycnals, like those in the above example, should be examined using the ageostrophic (primitive) equations—as has been done by Fukamachi et al. (1995). It would be interesting to examine if the nonlinearity of velocity and density profiles affects ageostrophic fronts as much as it does quasigeostrophic flows.

6. Conclusions

It has been demonstrated that the nonplanetary part of potential vorticity (anomalous vorticity) of oceanic currents is, typically, much greater than the planetary vorticity and, as a result, affects strongly the stability properties of the flow.

Vertical inhomogeneity of density stratification also affects baroclinic instability. Generally speaking, the stability properties of a flow are determined by its least stable layer (i.e., the layer with the weakest density gradient). Thus, *global* parameters (e.g., vertical density/velocity change through the active layer) are not representative of the stability properties of the flow, and the models ignoring its fine structure are too crude to capture the essential physics of instability.

Calculations based on the parameters of real-life currents in the northern Pacific demonstrate that the combined effect of nonzero anomalous vorticity and inhomogeneous density stratification can make baroclinic instability 2.5–6 times stronger and dramatically expand the spectral range of unstable disturbances toward the short-wave region (by a factor of more than 20–30). As a result, the parameters of baroclinic instability computed using linear approximation of density and velocity profiles (corresponding to constant density gradient and zero anomalous vorticity) differ considerably from those obtained through more realistic approximations.

Acknowledgments. This work was supported by Large Grant A39530698 of the Australian Research Council.

APPENDIX A

Derivation of (2)

It is worth noting that, when examining the eigenfunction in the homogeneous part of the basic flow, one

should resist the temptation to assume that it is determined by the hydrostatic pressure gradient and thus has a linear profile (this is, of course, correct for the basic flow, but not for the disturbance). Instead, we shall derive the structure of the disturbance from the standard boundary value problem for disturbances in a parallel flow on a β plane:

$$\frac{f^2 \rho_0}{g} \left[\frac{(u-c)^2}{\rho_z} \phi_z \right]_z + [k^2(u-c)^2 - \beta(u-c)] \phi = 0, \quad (\text{A1})$$

$$\phi_z = 0 \quad \text{at } z = 0, -H_0, \quad (\text{A2})$$

where the notation is explained in section 2. In order to derive a boundary condition describing a homogeneous passive layer, the simplest option would be to consider a uniformly stratified layer:

$$u(z) = 0, \quad \rho_z(z) = \rho' \quad \text{for } z \leq -H_a$$

and then take the limit $\rho' \rightarrow 0$. We shall choose, however, a more complicated but more general approach (which yields, of course, exactly the same result).

First, we shall rewrite Eq. (A1) in a form that would make the limit $\rho_z \rightarrow 0$ regular (in the equation's present form, this limit is singular). We shall integrate (A1) from $z = -H_0$ to $z = z'$ and take into account (A2):

$$\frac{f^2 \rho_0 [u(z') - c]^2}{g \rho_z(z')} \phi_z(z') + \int_{-H_0}^{z'} \{k^2[u(z) - c]^2 - \beta[u(z) - c]\} \phi(z) dz = 0. \quad (\text{A3})$$

Next we multiply (A3) by $g \rho_z(z') / f^2 \rho_0 [u(z') - c]^2$ and integrate from $z' = -H_0$ to $z' = z''$:

$$\begin{aligned} \phi(z'') = A - \int_{-H_0}^{z''} \frac{g \rho_z(z')}{f^2 \rho_0 [u(z') - c]^2} \\ \times \int_{-H_0}^{z'} \{k^2[u(z) - c]^2 - \beta[u(z) - c]\} \phi(z) dz dz', \end{aligned} \quad (\text{A4})$$

where $A = \phi(-H_0)$ (observe that, in view of linearity of the problem at hand, A plays the role of normalizing constant and, in principle, can be replaced with any particular number). Now our equation has become regular with respect to $u \rightarrow 0$, $\rho_z \rightarrow 0$. We shall take this limit in two steps: first we shall assume that, in the passive layer, u and ρ_z are small but finite, then we shall put $u = 0$, $\rho_z = 0$. Observe that, in the former case, the second term on the right-hand side of Eq. (A4) is small, while the first one remains finite. Thus, we can solve (A4) by iterations:

$$\begin{aligned} \phi(z'') &= A - \int_{-H_0}^{z''} \frac{g\rho_z'(z')}{f^2\rho_0[u(z') - c]^2} \\ &\times \int_{-H_0}^{z'} \{k^2[u(z) - c]^2 - \beta[u(z) - c]\} A dz dz' \\ &+ \dots \end{aligned} \tag{A5}$$

In order to match (A5) to the solution in the active layer, the continuity of the pressure and vertical velocity should be required. Calculating these quantities at the interface, we obtain

$$\begin{aligned} \phi(-H_a) &= A - \dots, \\ \frac{\phi_z(-H_a)}{\rho_z(-H_a)} &= \frac{g}{f^2\rho_0[u(-H_0) - c]^2} \\ &\times \int_{-H_0}^{H_a} \{k^2[u(z) - c]^2 - \beta[u(z) - c]\} A dz \\ &+ \dots \end{aligned}$$

Finally, putting $u = 0$, $\rho_z = 0$ and using the first equation to eliminate A , in the second equation, we obtain the desired boundary condition (2).

APPENDIX B Derivation of (7)

The active layer–passive layer interface will be treated here as an isopycnal surface. In order to derive an expression for the slope of isopycnal surfaces in a steady parallel flow, observe that the velocity, density, and pressure fields in it satisfy

$$\frac{1}{\rho_0} p_y = -fu, \tag{B1}$$

$$p_z = -g\dot{\rho}. \tag{B2}$$

We shall need an expression for ρ_y . To derive it, we differentiate (B2) with respect to y and take into account (B1):

$$\rho_y = \frac{f\rho_0}{g} u_z. \tag{B3}$$

The isopycnal surfaces are determined by

$$\rho(y, z) = \text{const},$$

and their slope is given by

$$z_y = -\frac{\rho_y}{\rho_z}. \tag{B4}$$

Substituting (B3) into (B4), we obtain

$$z_y = -\frac{f\rho_0}{g} \frac{u_z}{\rho_z}$$

as required.

REFERENCES

Benilov, E. S., 1994: The effect of continuous shear upon the two-layer model of baroclinic instability. *Geophys. Astrophys. Fluid Dyn.*, **78**, 95–113.

—, 1995: Baroclinic instability of quasi-geostrophic flows localized in a thin layer. *J. Fluid Mech.*, **288**, 175–199.

Charney, J. G., 1947: The dynamics of long waves in a baroclinic westerly current. *J. Meteor.*, **4**, 135–163.

Dormand, J. R., and P. J. Prince, 1980: A family of embedded Runge–Kutta formulae. *J. Comput. Appl. Math.*, **6**, 19–26.

Eady, E. T., 1949: Long waves and cyclone waves. *Tellus*, **1**, 33–52.

Fukamachi, Y., J. P. McCreary, and J. A. Proehl, 1995: Instability of density fronts in layer and continuously stratified models. *J. Geophys. Res.*, **100**, 2559–2577.

Gill, A. E., J. S. A. Green, and A. J. Simmons, 1974: Energy partition in the large-scale ocean circulation and the production of mid-ocean eddies. *Deep-Sea Res.*, **21**, 499–528.

Green, J. S. A., 1960: A problem in baroclinic stability. *Quart. J. Roy. Meteor. Soc.*, **86**, 237–251.

Hairer, E., S. P. Norsett, and G. Wanner, 1993: *Solving Ordinary Differential Equations 1: Nonstiff Problems*. Springer-Verlag, 528 pp.

Killworth, P. D., D. B. Chelton, and R. A. DeSzoeko, 1997: The speed of observed and theoretical long extratropical planetary waves. *J. Phys. Oceanogr.*, **27**, 1946–1966.

Lee, C. M., and C. C. Eriksen, 1996: The subinertial momentum balance of the North Atlantic subtropical convergence zone. *J. Phys. Oceanogr.*, **26**, 1690–1704.

Olson, D. B., 1991: Rings in the ocean. *Ann. Rev. Earth Planet. Sci.*, **19**, 283–311.

Pedlosky, J., 1987: *Geophysical Fluid Dynamics*. Springer-Verlag, 710 pp.

Phillips, N. A., 1954: Energy transformation and meridional circulation associated with simple baroclinic waves in a two-level, quasi-geostrophic model. *Tellus*, **6**, 273–286.

Roden, G. I., 1975: On the North Pacific temperature, salinity, sound velocity and density fronts and their relation to the wind and energy flux fields. *J. Phys. Oceanogr.*, **5**, 557–571.